# Hollow Core Double-Clad Fiber Coupler for Nonlinear Micro-Endoscopy

D. Septier, D. Labat, A. Pastre, R. Bernard, G. Brévalle-Wasilewski, Hervé Rigneault, Géraud Bouwmans, A. Kudlinski

# Hollow core double-clad fiber coupler for nonlinear micro-endoscopy

D. Septier[1,*], D. Labat[1], A. Pastre[1], R. Bernard[1], G. Brévalle-Wasilewski[2], H. Rigneault[2,3], G. Bouwmans[1], and A. Kudlinski[1]

[1]Univ. Lille, CNRS, UMR 8523 - PhLAM - Physique des Lasers Atomes et Molécules, F-59000 Lille, France
[2]Lightcore Technologies, Cannes, France
[3]Aix Marseille Univ, CNRS, Centrale Marseille, Institut Fresnel, Marseille, France
[*]dylan.septier@univ-lille.fr

**Abstract:** We report the design, fabrication and characterization of the first hollow core double-clad fiber coupler for nonlinear micro-endoscopy. It is made of a pure silica negative curvature hollow core double-clad fiber and a highly multimode fiber fused along each other. The fabrication of such a coupler was made possible thanks to the use of a soft (borosilicate) glass multimode fiber which can be fused along the negative curvature fiber without altering its geometry, thanks to its much lower fusion temperature. A 60% power transfer from the double-clad fiber to the multimode one was measured at 500 nm. Demonstration of nonlinear imaging was performed on unlabeled biological tissues with an endoscopic head mounted on the hollow core double-clad fiber coupler to demonstrate its applicability. This device greatly simplifies the integration of nonlinear micro-endoscopes based on hollow core double clad fibers.

## 1. Introduction

There has been a growing interest in nonlinear micro-endoscopy over the past decade [1], following the rapid progress in compact ultrafast lasers and specialty optical fibers. In a typical nonlinear micro-endoscopy setup [see Fig. 1(a)], ultrashort pulses are launched in an optical fiber and delivered onto a sample in order to excite its nonlinear response (multiphoton absorption, harmonic generation or stimulated Raman scattering). The nonlinear signal must be collected and sent to the detection channel through an optical fiber. One possibility is to use a collection fiber different from the excitation one [2–5]. In this case, the collected nonlinear signal can be easily sent to the detection, but the design of the endoscopic head is complicated and makes it rather large (typically close to 10 mm diameter), which is not ideal for endoscopic applications. Another option is to collect the nonlinear signal through the excitation fiber itself, by using a double-clad fiber (DCF) [6–13]. The distal head is much simpler and much more compact, because a single optical fiber is used. In this case, the central core is used to deliver the exciting ultrashort pulses, and the surrounding cladding is used to collect the nonlinear signal generated within the sample. At the fiber input, the collected signal is separated from the exciting one with a dichroic mirror placed between the injection lens and the fiber [see Fig. 1(a)]. This causes several problems: (i) it restricts the focal length of the injection lens to values typically larger than a few tens of mm, because of the size of the dichroic mirror, (ii) this makes the alignment very delicate, time-consuming and (iii) prone to misalignment due to environmental perturbations, which can degrade the overall performances of the system even during imaging sessions. It is therefore crucial to reduce this sensitivity to external perturbations in view of using the endoscope outside a laboratory environment.

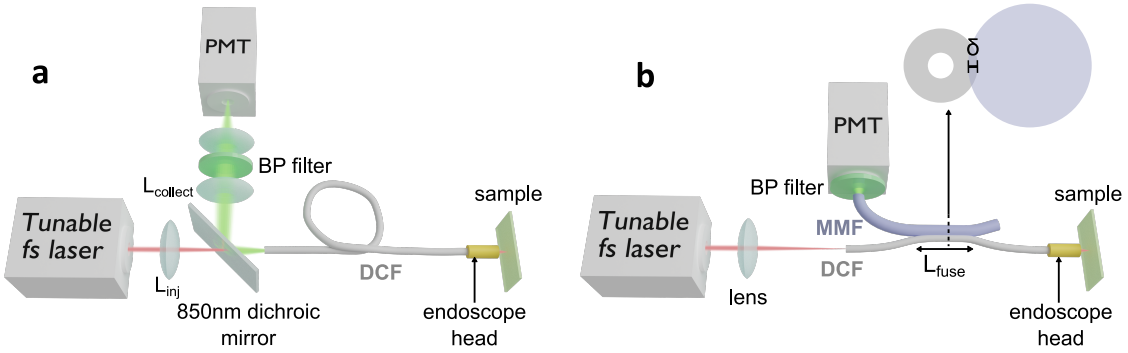


**Figure 1:** *Typical nonlinear endoscopy scheme setup based on a hollow core DCF. Excitation and collected signal, respectively guided through the hollow core and the silica clad, are separated either with (a) a dichroic mirror or (b) a double-clad fiber coupler.*

In this scope, DCF couplers have been developed to separate signals from the core and the inner cladding of solid-core double-clad fibers [11, 14–16]. They are all-fiber components in which pulses are delivered to the sample through a single-mode core and the collected light is extracted from the silica cladding and transferred to another fiber, which is fused along the delivering fiber [17]. For two fibers with identical diameter, the theoretical light transfer from one multimode cladding to the other is limited to 50% [17]. Asymmetric DCF couplers allow improving it [18] leading to the demonstration of a transfer rate as high as 80% [19]. Such components greatly simplify nonlinear endoscopy setups [see Fig. 1(b)] as they allow avoiding the use of a dichroic mirror with all of its disadvantages listed above. They have been used for spectrally encoded endoscopy [17, 18], confocal fiber-based microscopy [19] or nonlinear micro-endoscopy [11, 16].

Recently, hollow core fibers have emerged as a promising platform for nonlinear micro-endoscopy or spectroscopy thanks to their ability to deliver intense and ultrashort pulses with very limited distortions [12, 20, 21]. Naturally, hollow-core DCFs have been developed and successfully used to demonstrate flexible nonlinear micro-endoscopes [8, 10, 12, 13]. In particular, negative curvature hollow core DCFs allow avoiding the use of dispersion and/or nonlinearity pre-compensation schemes, which greatly simplifies the experimental setup. However, similarly to the scheme of Fig. 1(a), a dichroic mirror is still required to separate excitation and collection signals.

In this paper, we demonstrate the fabrication and characterization of an negative curvature hollow-core DCF coupler. It is based on a silica negative curvature hollow core fiber and a coreless borosilicate glass (BG) multimode fiber (MMF). The much lower fusion temperature of the BG as compared to pure silica allow fabricating the component without affecting the microstructure of the tubular hollow-core fiber. We demonstrate its use for nonlinear micro-endoscopy using the setup of Fig. 1(b) and compare its efficiency with a standard detection setup using a dichroic mirror.

## 2. Coupler design and simulations

As stated above, the primary aim of the hollow core DCF coupler designed here is to be integrated in a nonlinear endoscopy setup in order to replace the standard dichroic mirror for the separation of the excitation and collected signals propagating respectively in the core and inner cladding of the DCF. Figure 1(a) is a schematic representation of this typical setup. Because the numerical aperture (NA) of the core (≈0.02) and inner cladding (≈0.38) of the

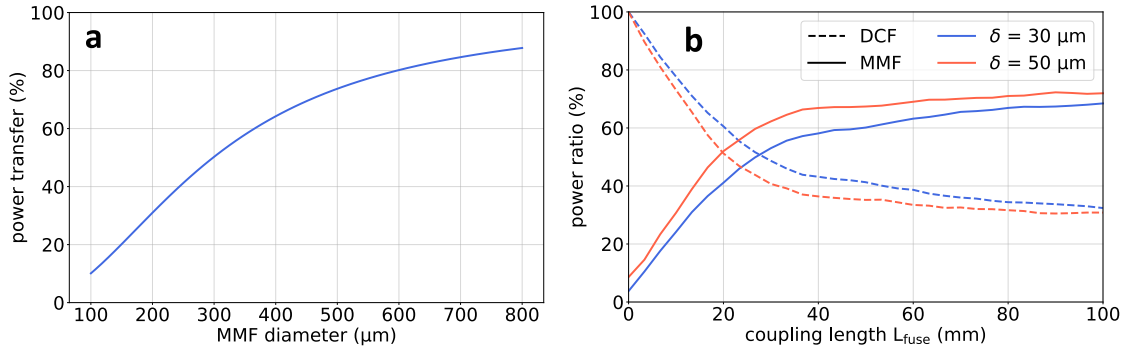


**Figure 2:** *(a) Power transfer from a hollow core DCF to a MMF as a function of MMF diameter for a 300 µm outer diameter hollow core DCF, calculated using Eq. 1 [18]. (b) Numerical simulations of the power distribution inside the hollow core DCF (dashed lines) and MMF (solid lines) as a function of coupling length, for overlap parameter values of $\delta = 30$ µm (blue lines) and $\delta = 50$ µm (red lines).*

hollow core DCF are separated by an order of magnitude [12], different lenses have to be used (i) to inject light into the core and (ii) to collect light from the double-clad and redirect it to the detector. Therefore, the dichroic mirror must be placed between the injection lens [labeled $L_{\mathrm{inj}}$ in Fig. 1(a)] and the fiber, making the placement and alignment delicate and time-consuming. Moreover, it needs to be readjusted on a regular basis to keep the collection optimized. Whereas this is not a major drawback when aligning the setup in a lab, it can get problematic in clinic applications where the endoscope needs to be readily available at any time. For these reasons, replacing the bulk optics by a hollow core DCF coupler, as represented in Fig.1 (b), would improve the robustness of the setup alignment while greatly simplifying it.

Based on previously mentioned studies, we chose an asymmetric design for the coupler to maximize the power transfer from the double-clad of the DCF to the MMF. In [18], an analytical formula is presented to calculate the MM transfer in such a design, based on the optical etendue calculation $G = \pi S(\mathrm{NA})^2$, with NA the numerical aperture of the DCF double-clad, and $S$ its surface. The transfer from the DCF to the MMF is then calculated as [18]:

$$T = \frac{G_{\mathrm{MMF}}}{G_{\mathrm{MMF}} + G_{\mathrm{DCF}}} \tag{1}$$

where $G_{\mathrm{DCF}}$ and $G_{\mathrm{MMF}}$ are respectively the etendue of the DCF double-clad and of the MMF, assuming that they have the same NA. Using this formula, the transfer from a DCF of fixed 300 µm outer diameter to a MMF of varying outer diameter is calculated and represented in Fig.2(a). As expected, a 50% transfer is obtained with a symmetrical design, but it gets higher as the MMF diameter increases. We chose a 500 µm outer diameter MMF as it gives a good compromise of flexibility and solidity during its manipulation and an acceptable transfer expected to be about 70%. Regarding the fabrication process, two parameters have a significant impact on the overall performances of the coupler: the coupling length, *i.e.* the length over which the fibers will be spliced (labeled $L_{\mathrm{fuse}}$), and the overlap parameter (labeled $\delta$) which corresponds to the overlap distance between the fibers outer edge in the spliced area [see inset of Fig.1(b)].

Additionally, we performed beam propagation method (BPM) simulations using a finite element method [22] to calculate the power distribution in both fibers as a function of the coupling length. Calculations were realized for 2000 modes at the input of the DCF double clad, with a propagation step of 0.5 µm, assuming both fibers are made of silica, and at a wavelength of 500 nm. Figure 2(b) shows the power distribution remaining in the DCF (dashed lines) and transferred to the MMF (solid lines), for two realistic overlap parameter values of

$\delta = 30$ µm (blue lines) and $\delta = 50$ µm (red lines). In both cases, we see an exchange in power from the DCF to the MMF during the 40 mm of the coupler, followed by a stabilization of the power in each fiber to an almost constant value. The power in the MMF reaches 69% for $\delta = 30$ µm and 72% for $\delta = 50$ µm after a length of 100 mm, confirming the results of about 70% obtained from the analytical model (Eq. 1). For a greater overlap parameter, this value remains almost unchanged, but it is reached for a shorter coupling length (results not shown here).

## 3. Fabrication

The main challenge for the fabrication of the hollow core DCF coupler designed in the previous section is to keep the structure of the negative curvature hollow core fiber intact. Indeed, the transmission properties of the fiber are fixed by the ring of capillaries surrounding the hollow core [23, 24]. In particular, the capillary thickness fixes the spectral location of transmission bands, and their spacing has a strong impact on the fiber attenuation [25]. It is therefore crucial not to distort the overall capillary structure during the fabrication of the coupler.

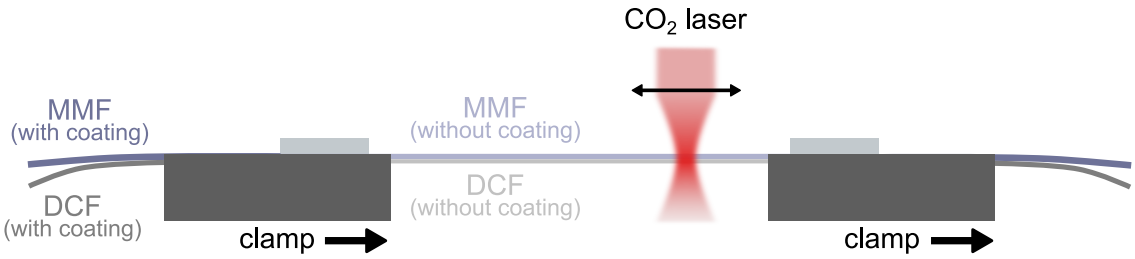


**Figure 3:** *DCF coupler fabrication setup. Fibers, stripped of their coating, are clamped against each other and fused using a $CO_2$ laser.*

To do that, we use a fusion process in order to fuse the fibers side by side longitudinally, with a commercially available glass processing and fusion system based on a $CO_2$ laser heat source (Fujikura LZM-100). No tapering can be performed for the reasons explained above, as opposed to previously reported studies [16–19]. Prior to the fusion stage, the coating of both fibers is removed over a 20 cm length. They are then placed on top of each other and clamped in two V-grooves separated by about 15 cm, as depicted in Fig. 3. A part of the section of the bare fibers located in between the V-grooves is then scanned with the $CO_2$ laser beam with appropriate speed (0.14 µm/ms) and heating power (typically 3 to 15 µW), which results in their fusion over this distance. Afterwards, the whole component is re-coated using a homemade system with a low index polymer in order to ensure guidance of the MMF, and protection.

Our preliminary fabrication tests were made using a 500 µm MMF made of a pure silica glass rod surrounded by a low index polymer, in order to ensure multimode guidance in the rod. The DCF was a pure silica capillary with inner and outer diameters equal to the ones of the negative curvature fiber to be used eventually (of respectively 70 and 300 µm), also surrounded by a low index polymer coating. The couplers fabricated during these preliminary tests were intended to be destroyed in order to be characterized, which is why we used capillary fibers instead of high quality negative curvature fibers. At first, we fixed the coupling length to $L_{\text{fuse}} = 20$ mm and studied the impact of heating power on the overlap parameter $\delta$. Each of the fabricated coupler was then cut and cleaved in the fusion section in order to measure the

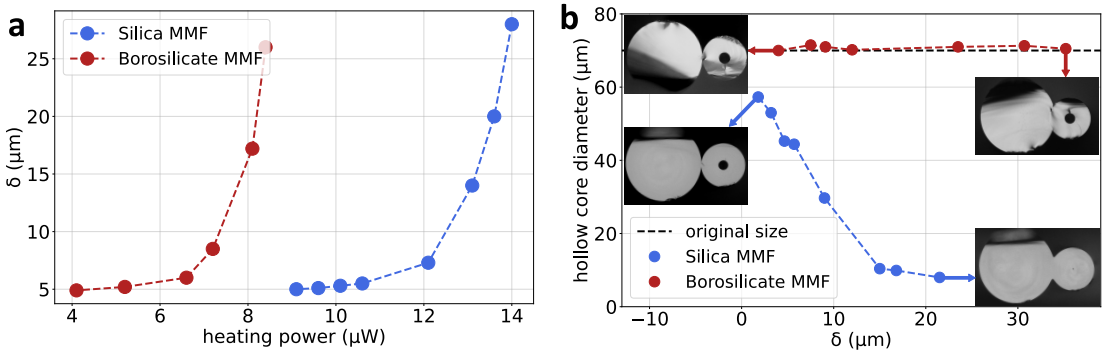


**Figure 4:** *(a) Measured overlap parameter $\delta$ between the DCF and the MMF as a function of the $CO_2$ laser heating power, using a pure silica MMF (blue dots) and a BG MMF (red dots). (b) Measured capillary inner diameter as a function of the overlap between the fibers using a pure silica MMF (blue dots) and a BG MMF (red dots). The horizontal black dashed line depicts the initial inner diameter of the capillary fiber.*

overlap parameter in the transverse structure under a microscope. The results are depicted by blue markers in Fig. 4(a), which shows that the overlap increases with heating power and reaches 28 μm for 14 μW. However, for every heating power between 9 and 14 μW, a significant collapse of the capillary central hole was observed. Figure 4(b) shows the capillary inner diameter measured after the fabrication process as a function of the overlap between both fibers (blue dots). From an initial 70 μm value, the inner hole almost completely collapses for an overlap of 20 μm [see corresponding photo in inset of Fig. 4(b)]. In fact, even for a very small overlap of 2 μm, being the smallest value obtained while keeping the fibers fused, we measured that the inner capillary diameter has already decreased from 70 to 57 μm. This is a major issue since the capillary fiber is intended to be replaced by an negative curvature hollow-core fiber and no distortion from the structure can be tolerated as explained above.

To overcome this issue, we performed a second series of tests by replacing the pure silica MMF with a MMF made of a glass material having a much lower fusion temperature than silica. Additionally, its refractive index must be higher than the pure silica one, in order to maximize the mode transfer from the DCF to MMF and to ensure guidance and high NA when the fiber is coated with a low index polymer. Borosilicate glasses are adequate and low-cost candidates for that. We chose here a Simax glass [26] with a melting point of 820°C (far lower than the silica one of 1710°C) and a refractive index of 1.478 at 500 nm (higher than the silica one of 1.462 at 500 nm). We fabricated 500 μm BG MMFs coated with low index polymer, and we repeated the same run of experiments as for the pure silica MMF. The results are reported with red markers in Figs. 4(a) and (b). Figure 4(a) shows that overlap values between 5 and 30 μm can be obtained for heating powers between 4 and 8.5 μW, much lower than for the silica MMF. More importantly, Fig. 4(b) demonstrates that for overlap values up to 30 μm, no reduction of the inner capillary diameter is observed, because the temperature required to soften the MMF glass is much lower than the melting point of pure silica. This suggests that such components can be fabricated with real negative curvature fibers without affecting their microstructure nor their transmission properties.

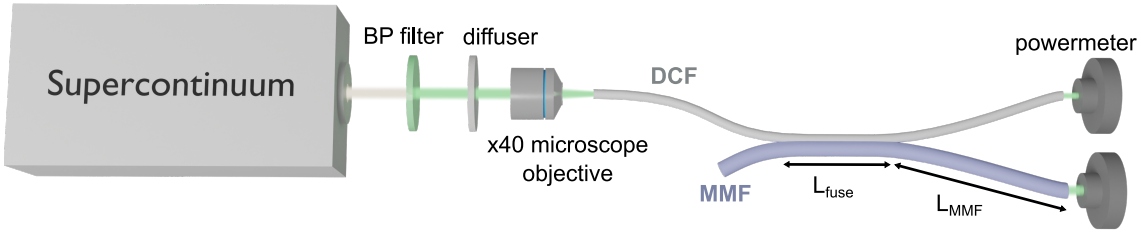


**Figure 5:** *Hollow-core DCF coupler characterization setup. A supercontinuum is injected into the silica clad of the hollow-core DCF, and a bandpass (BP) filter allows choosing the target wavelength. A diffuser coupled with a high numerical aperture (NA = 0.65) microscope objective insures the excitation of all guided modes of the silica clad.*

# 4. Optical characterization

## 4.1. Measurement of the power transfer

In order to reach an optimized process to fabricate a DCF coupler that maximizes the power transfer from the double clad of the hollow core DCF to the MMF, we performed a succession of fabrications and characterizations using once again a 300 µm outer diameter and 70 µm inner diameter silica capillary fiber (DCF) and a 500 µm outer diameter BG rod (MMF). After fabrication, the power transfer was measured using the setup shown in Fig. 5. A homemade supercontinuum covering the whole visible range with a set of 10 nm wide bandpass filters allowed us to address individual wavelengths. A $\times$40 microscope objective with a high numerical aperture (NA = 0.65) preceded with an optical diffuser allowed excitation of all modes guided inside the double clad of the capillary fiber, of measured numerical aperture NA = 0.38. Fibers lengths are kept equal for all measurements, before and after the splice, to guarantee a comparison unaffected by propagation loss. The average power measured at the output of both fibers is then compared to the power measured in the DCF 10 cm before the splice, granting a relative power transfer measurement.

Figure 6(a) shows the power transfer for a wavelength of 500 nm to the MMF as a function of the splice length $L_{\text{splice}}$, for a fixed overlap parameter $\delta = 15$ µm, and with a 15 cm length of each fiber after the spliced area. We observe an increase of the MM transfer in the first 20 mm of coupling, and an almost constant value, slightly under 50%, for coupling lengths above 20 mm. A similar behavior is obtained in Fig. 6(b) when fixing $L_{\text{splice}} = 25$ mm and varying the overlap between fibers. The power transfer is almost constant, with a sharp decrease for overlaps smaller than 7 µm. From these trend, we can safely conclude that for a spliced length of 20 to 50 mm and an overlap of 10 to 30 µm we should obtain similar performances, maximizing the power transfer to the BG MMF. For all subsequent results, we chose an overlap of $\delta = 15$ µm and a spliced length $L_{\text{splice}} = 25$ mm.

Although the use of a BG MMF allowed us to fuse the two fibers together without affecting the hollow core DCF hollow structure, its propagation losses in the visible range remain a major issue. Propagation losses in the 500 µm outer diameter BG rod are measured to be around 10 dB/m in the spectral range of interest. Figure 6(c) displays the power transfer at the output of the BG MMF for a fiber length $L_{\text{MMF}} = 10$ cm (dark blue dots) and $L_{\text{MMF}} = 15$ cm (light blue dots) after the spliced area. Shrinking the BG fiber length greatly improves the power transfer obtained by minimizing the impact of its propagation losses. We found that $L_{\text{MMF}} = 10$ cm is the shortest length we could obtain while still being able to manipulate the coupler and separate the two fibers without risking to break them, and gives satisfying results, with a power transfer of about 60%.

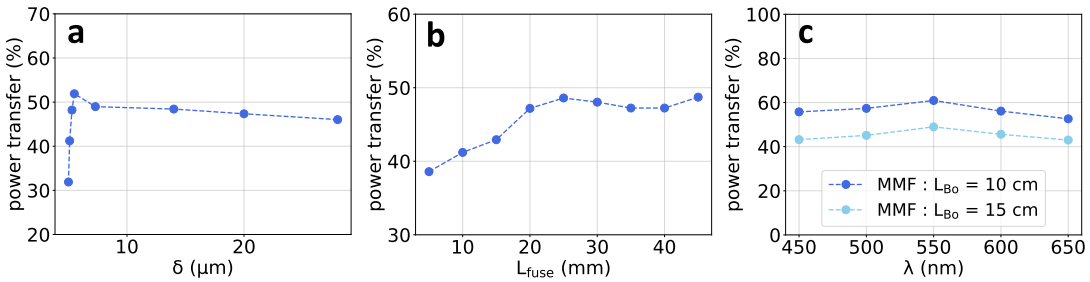


**Figure 6:** *Measured power transfer of a hollow-core DCF coupler with a 300 μm outer diameter hollow core DCF and a 500 μm outer diameter BG MMF as a function of (a) the coupler length $L_{fuse}$ and (b) the overlap parameter $\delta$ between both fibers. (d) Measured power transfer after 15 cm (light blue dots) or 10 cm (dark blue dots) of propagation inside the BG MMF after the coupler.*

## 4.2. Transmission properties

Now that we have optimized the power transfer from the cladding of the DCF to the MMF, the next step is to fabricate a coupler with an negative curvature hollow core DCF and to show that the transmission properties of the hollow core are not affected by the coupler fabrication. To do that, we used the negative curvature hollow core DCF displayed in Fig. 7(a). The hollow core is 34 μm in diameter and is surrounded by 7 capillaries of 13.1 μm outer diameter and 0.35 μm wall thickness. The measured mode field diameter (MFD) of the fundamental mode is 30.5 μm. The first transmission band goes from 800 nm to more than 1750 nm with propagation losses of about 0.6 dB/m over the whole transmission band (not shown here).

A coupler was fabricated using this fiber and a 500 μm BG MMF following the fabrication procedure described above. Figure 7(c) shows a scanning electron microscope (SEM) image taken by cutting the coupler in its fused section, after optical characterization had been done. From this image, the overlap parameter $\delta$ is estimated to be $\delta = 26$ μm. A detailed comparison of the geometrical parameters of the DCF structure before [Fig. 7(a)] and after [Fig. 7(c)] the coupler fabrication showed that no noticeable deformations were induced by the fusion process.

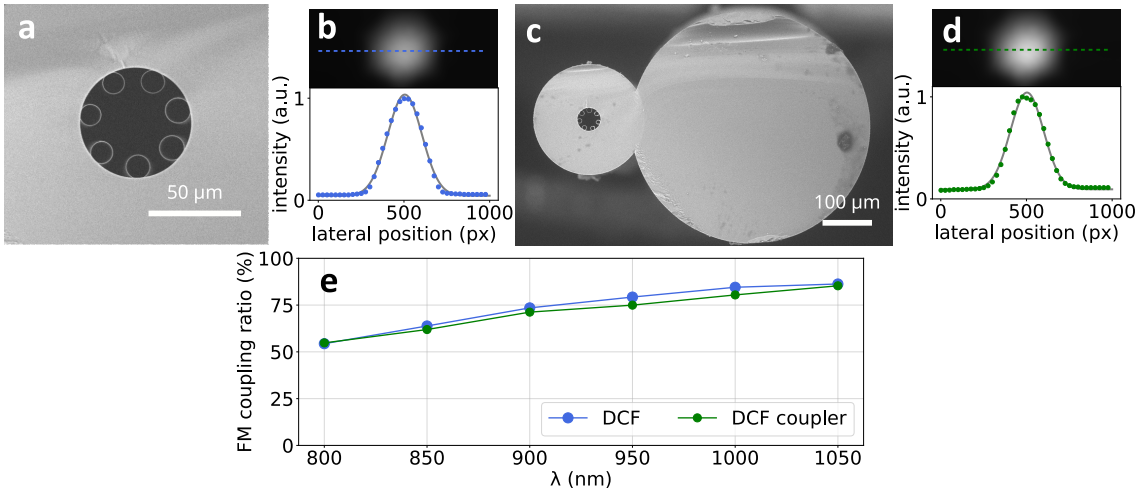


**Figure 7:** *SEM of (a) the 7 capillary hollow core DCF and (c) the hollow core DCF coupler fabricated with it and a 500 μm outer diameter BG MMF. Imaged hollow core FM of the hollow core DCF (b) before and (d) after fabrication of the coupler, with a profile plot along the marked horizontal dashed line and a Gaussian fit (gray solid line). (e) Hollow core fundamental mode coupling ratio of the hollow core DCF before (blue dots) and after (green dots) fabrication of the coupler.*

This is confirmed by measuring and comparing the fundamental mode profile in the hollow core before [Fig. 7(b)] and after [Fig. 7(d)] the coupler fabrication. A nearly Gaussian profile is obtained in both cases, with a $1/e^2$ diameter of 399 pixels before the fusion process [Fig. 7(b)] and of 387 pixels after [Fig. 7(d)].

Finally, we compare in [Fig. 7(e)] the injection rate into the negative curvature hollow core DCF before (blue markers) and after (green markers) fusing the BG MMF. To do that, we used a tunable Ti:Sa laser delivering 200 fs pulses at 80 MHz launched into the hollow core of the DCF with a lens of 30 mm focal length. The injection rate is defined as the power out of a short fiber piece ($< 1$ m) over the available power after the coupling lens. The results of Fig. 7(e) show that the injection rate between 800 and 1050 nm is almost identical (within the measurement uncertainty) before and after the fusion process, confirming that the coupler fabrication does not affect the transmission efficiency of the hollow core DCF. Note that the wavelength dependence of the injection rate (from 55 % at 800 nm to 85 % at 1050 nm) is due to the fact that the coupling lens was not optimized for all wavelengths.

# 5. Demonstration of nonlinear imaging

## 5.1. Collection efficiency

Because the purpose of the hollow core DCF coupler proposed here is to simplify nonlinear endoscopy setups, we performed a direct comparison of the collection efficiency of the 2-photon excited fluorescence (2PEF) signal using a setup with a dichroic mirror [Fig. 1(a)] and with the hollow core DCF coupler [Fig. 1(b)]. The excitation laser is a Ti:Sa oscillator (Chameleon, Coherent) delivering 200 fs pulses tuned at 920 nm, at the repetition rate of 80 MHz. In a first experiment, it was injected in a 2 m long hollow core DCF similar to the one of Fig. 7(a) with a 30 mm focal lens. No distal optics was used at the fiber output. The sample (a calibration fluorescent slide) was placed directly 100 µm away from the fiber endface. The 2PEF signal was collected by the fiber double-clad and redirected to the detection channel by the dichroic mirror (Semrock FF850-Di01-t1-25x36) placed at the fiber input [see Fig. 1(a)] and a collecting lens. The 2PEF signal was filtered by a 565±66 nm bandpass filter and focused on the photomultiplier tube (PMT). Figure 8(a) shows the collected signal as a function of the excitation power on the fluorescent slide measured using this setup (blue markers). It has the expected quadratic dependence with the excitation power (solid line) and reaches 5.3 M count/s for 30 mW.

In a second experiment, we used the same hollow core DCF sample, and we fabricated a coupler with a 500 µm diameter BG MMF. The coupler parameters were $\delta = 20$ µm, $L_{\text{fuse}} = 25$ mm and $L_{\text{MMF}} = 10$ cm, in accordance with the optimization rules describes above. This fabricated coupler was then placed in the experimental setup represented in Fig. 1(b) (the dichroic mirror, collimating lens and focusing lens of the detection channel were removed). The output light MMF port of the coupler was sent directly on the bandpass filter placed in front of the PMT. Green markers in Fig. 8(b) represent the evolution of 2PEF collected signal as a function of excitation power. It shows a quadratic dependence (solid line) and reaches 3.9 M count/s for 30 mW, which is about 20% lower than what was obtained with the more standard setup using the dichroic mirror. This slightly lower collection efficiency of the hollow core DCF coupler is presumably due to the high loss (of 10 dB/m) of the BG MMF used to fabricate the component, and could be improved using a lower attenuation glass. It is however high enough to perform nonlinear imaging, as we shall see in the following.

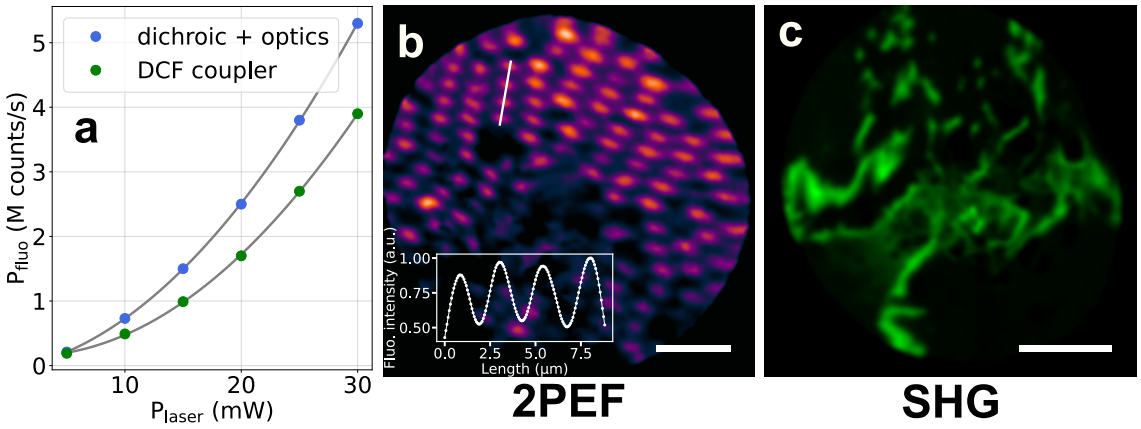


**Figure 8:** *(a) 2PEF signal generated inside a fluorescent slide at the output of the hollow core DCF for an excitation wavelength $\lambda_{exc} = 920$ nm as a function of the excitation power. The collected signal is separated from the excitation either by a dichroic mirror and appropriate optics (blue dots) or by a hollow core DCF coupler with a 500 μm outer diameter BG MMF (green dots). (b) 2PEF image of 2 μm fluorescent beads with an intensity plot along the white line ($\lambda_{exc} = 920$ nm). Scale bar is 20 μm. (c) SHG image of unstained mouse skin ($\lambda_{exc} = 920$ nm). Scale bar is 50 μm. Images have been acquired with a 2 fps acquisition rate and averaged over 5 images.*

### 5.2. Implementation in a nonlinear endoscopic imaging setup

In order to illustrate the ability to use this hollow core DCF coupler in a nonlinear endoscopic imaging setup, we mounted a full endoscopic head at the output of the DCF port of the coupler. It is similar to the one detailed in [13]. Briefly, it is composed of a 60 μm core diameter germanium-doped GRIN fiber with a 160 μm length spliced to the hollow core DCF output. The fiber is placed into a doubly resonant piezoelectric tube (Physik Instrumente) in order to provide a resonant excitation of the fiber tip that follows a spiral pattern. A miniature GRIN objective (GRINTECH GmbH GT-MO-070- 016-ACR-VISNIR-30-20) is used to image the output spot of the fiber onto the sample. The field of view on the sample is up to 200 μm. These components are set inside a 3 mm outer diameter and 35 mm long bio-compatible stainless steel tube.

We first demonstrate in Fig. 8(b) nonlinear imaging with a 2PEF image of 2 μm fluorescent beads, with an insight showing an intensity plot along the white line. The excitation wavelength is $\lambda_{exc} = 920$ nm and a 565±66 nm bandpass filter is used to isolate the 2PEF signal. We further highlight the imaging potential of the present device with a biological image of unstained mouse skin using second harmonic generation (SHG) imaging in Fig. 8(c). Collagen fibrils, known to emit a strong SHG signal, are identifiable. In this case, the excitation is identical to 2PEF imaging, $\lambda_{exc} = 920$ nm, and a 447±60 nm bandpass filter ensures the collection of SHG signal only. These experiments demonstrate that the developed hollow core DCF coupler can successfully replace the dichroic mirror, making the endoscopy setup more reliable.

## 6. Conclusion

We developed a hollow core DCF coupler dedicated to nonlinear endoscopic applications. The use of two fibers of different glasses, namely silica and borosilicate, allowed us to develop a fusion based fabrication process which does not affect the delicate tubular structure of negative curvature hollow core fibers. The asymmetric design of the coupler allows reaching a power

transfer of 60 % from the double-clad of the DCF to the MMF. We implemented the coupler in a nonlinear endoscopy setup, making it much simpler and more robust to misalignment. Finally, we demonstrated its ability to perform efficient 2PEF and SHG imaging.

## References


1. Kučikas, V., Werner, M. P., Schmitz-Rode, T., Louradour, F. & van Zandvoort, M. A. M. J. Two-Photon Endoscopy: State of the Art and Perspectives. *Molecular Imaging and Biology* (Nov. 2021).
2. Balu, M., Liu, G., Chen, Z., Tromberg, B. J. & Potma, E. O. Fiber Delivered Probe for Efficient CARS Imaging of Tissues. *Optics Express* **18,** 2380–2388 (Feb. 2010).
3. Smith, B. *et al.* Portable, Miniaturized, Fibre Delivered, Multimodal CARS Exoscope. *Optics Express* **21,** 17161–17175 (July 2013).
4. Dochow, S. *et al.* Combined Fiber Probe for Fluorescence Lifetime and Raman Spectroscopy. *Analytical and bioanalytical chemistry* **407,** 8291–8301 (Nov. 2015).
5. Lukic, A. *et al.* Endoscopic Fiber Probe for Nonlinear Spectroscopic Imaging. *Optica* **4,** 496–501 (May 2017).
6. Zhao, Y., Nakamura, H. & Gordon, R. J. Development of a Versatile Two-Photon Endoscope for Biological Imaging. *Biomedical Optics Express* **1,** 1159–1172 (Nov. 2010).
7. Rivera, D. R. *et al.* Compact and Flexible Raster Scanning Multiphoton Endoscope Capable of Imaging Unstained Tissue. *Proceedings of the National Academy of Sciences* **108,** 17598–17603 (Oct. 2011).
8. Ducourthial, G. *et al.* Development of a Real-Time Flexible Multiphoton Microendoscope for Label-Free Imaging in a Live Animal. *Scientific Reports* **5,** 1–9 (Dec. 2015).
9. Liang, W., Hall, G., Messerschmidt, B., Li, M.-J. & Li, X. Nonlinear Optical Endomicroscopy for Label-Free Functional Histology in Vivo. *Light: Science & Applications* **6,** e17082–e17082 (Nov. 2017).
10. Lombardini, A. *et al.* High-Resolution Multimodal Flexible Coherent Raman Endoscope. *Light-Science & Applications* **7,** 10 (May 2018).
11. Akhoundi, F., Qin, Y., Peyghambarian, N., Barton, J. K. & Kieu, K. Compact Fiber-Based Multi-Photon Endoscope Working at 1700 Nm. *Biomedical Optics Express* **9,** 2326–2335 (May 2018).
12. Kudlinski, A. *et al.* Double Clad Tubular Anti-Resonant Hollow Core Fiber for Nonlinear Microendoscopy. *Optics Express* **28,** 15062–15070 (May 2020).
13. Septier, D. *et al.* Label-Free Highly Multimodal Nonlinear Endoscope. *Optics Express* **30,** 25020–25033 (July 2022).
14. Wang, L., Choi, H. Y., Jung, Y., Lee, B. H. & Kim, K.-T. Optical Probe Based on Double-Clad Optical Fiber for Fluorescence Spectroscopy. *Optics Express* **15,** 17681–17689 (Dec. 2007).
15. Ryu, S.-Y. *et al.* The Development of Double Clad Fiber and Double Clad Fiber Coupler for Fiber Based Biomedical Imaging Systems. *Journal of the Optical Society of Korea* **13,** 310–315 (Sept. 2009).
16. Bao, H., Ryu, S. Y., Lee, B. H., Tao, W. & Gu, M. Nonlinear Endomicroscopy Using a Double-Clad Fiber Coupler. *Optics Letters* **35,** 995–997 (Apr. 2010).

17. Lemire-Renaud, S. *et al.* Double-Clad Fiber Coupler for Endoscopy. *Optics Express* **18,** 9755–9764 (May 2010).

18. Madore, W.-J. *et al.* Asymmetric Double-Clad Fiber Couplers for Endoscopy. *Optics Letters* **38,** 4514–4517 (Nov. 2013).

19. Montigny, E. D. *et al.* Double-Clad Fiber Coupler for Partially Coherent Detection. *Optics Express* **23,** 9040–9051 (Apr. 2015).

20. Wang, Y. Y. *et al.* Design and Fabrication of Hollow-Core Photonic Crystal Fibers for High-Power Ultrashort Pulse Transportation and Pulse Compression. *Optics Letters* **37,** 3111–3113 (Aug. 2012).

21. Kolyadin, A. N. *et al.* Negative Curvature Hollow-core Fibers: Dispersion Properties and Femtosecond Pulse Delivery. *Physics Procedia. 4th International Conference of Photonics and Information Optics, PhIO 2015, 28-30 January 2015, Moscow, Russian Federation* **73,** 59–66 (Jan. 2015).

22. Koshiba, M., Hayata, K. & Suzuki, M. Approximate Scalar Finite-Element Analysis of Anisotropic Optical Waveguides. *Electronics Letters* **18,** 411–413 (May 13, 1982).

23. Pryamikov, A. D. *et al.* Demonstration of a Waveguide Regime for a Silica Hollow - Core Microstructured Optical Fiber with a Negative Curvature of the Core Boundary in the Spectral Region > 3.5 $M$m. *Optics Express* **19,** 1441–1448 (Jan. 2011).

24. Wei, C., Weiblen, R. J., Menyuk, C. R. & Hu, J. Negative Curvature Fibers. *Advances in Optics and Photonics* **9,** 504–561 (Sept. 2017).

25. Debord, B. *et al.* Ultralow Transmission Loss in Inhibited-Coupling Guiding Hollow Fibers. *Optica* **4,** 209–217 (Feb. 2017).

26. *Pegasus Glass : SIMAX Technical Information* https://www.pegasus-glass.com / Portals / 0 / technical_info.pdf.